Supporting Information

Lobsiger et al. 10.1073/pnas.1318309110

SI Materials and Methods

Animals. All transgenic mouse lines were on a pure C57BL/6J background. Transgenic mutant superoxide-dismutase 1 ($SOD1^{G37R}$) (line 42) ALS mice (6-mo average survival), that were previously generated in our laboratory and that express a 12-kb genomic DNA fragment encoding the human *SOD1G37R* transgene under its endogenous promoter, were used as heterozygous ($SOD1^{G37R}$) (1)." *C1qa* KO mice ($C1q^{-/-}$) were initially generated by Marina Botto (Imperial College London, London, United Kingdom) (2). With her permission, they were provided by Ben Barres (Stanford Univeristy, Stanford, CA). Although C1q-deleted mice lack classic complement pathway activation and would be thus more sensitive to foreign pathogens, this does not result in an overt deleterious immunodeficiency when mice are kept in standard pathogen-free conditions (3). To obtain C1q-deleted ALS mice, we crossed $SOD1^{G37R}$ with $C1q^{-/-}$ mice to obtain double-heterozygous animals, which were then bred to $C1q^{+/-}$ mice to obtain the final three genotypes, $SOD1^{G37R}/C1q^{+/+}$, $SOD1^{G37R}/C1q^{+/-}$, and $SOD1^{G37R}/C1q^{-/-}$, with expected Mendelian ratios. Control mice overexpressing high levels of human WT SOD1 ($SOD1^{WT}$, line 76) were used as heterozygous ($SOD1^{WT}$) (1). *C3* KO mice (homozygous; no. 003641) and ALS mice expressing $SOD1^{G93A}$ (Gur/J; heterozygous; no. 002726) were purchased from the Jackson Laboratory and bred as described for $SOD1^{G37R}$/C1q. All animal experiments used in this work were approved by the Animal Care and Use Committee of the University of California, San Diego.

Analysis of Disease Progression in ALS Mice. Mice were weighed weekly to provide an objective and unbiased measure of disease course, as described previously (1, 4, 5). Briefly, time of disease "onset" was retrospectively determined as the time when mice reached peak body weight. The time of progression to "early disease" was defined as the time when disease-induced weight loss had produced a 10% loss of maximal weight (which is accompanied by gait alterations and failure of hindlimb splaying reflex, without obvious signs of paralysis). This early disease stage is followed by the appearance of progressive paralysis. During the symptomatic phase, mice were observed daily, and "end stage" was defined by paralysis so severe that the animal could not right itself within 20 s when placed on its side, an endpoint frequently used for ALS mice and one that was consistent with the requirements of the Animal Care and Use Committee of the University of California, San Diego. Survial analysis was done using Kaplan–Meier survival curves, and statistically significant changes were determined by a log-rank test and Student *t* test (Prism version 4; GraphPad).

Disease Stage-Specific Tissue Collection. Three disease stages were chosen for RNA measurements by using real-time RT-PCR and immunohistochemical analysis (motor neuron number, neuroinflammation, synaptic density) of ALS mice ($SOD1^{G37R}/C1q^{+/+}$ and $SOD1^{G37R}/C1q^{-/-}$). For presymptomatic disease stages, mice were used at 8 wk of age, a time point without obvious symptoms and minimal motor neuron degeneration (1). For onset disease stages, mice were taken at 18 wk (the average age when reaching weight peak). For end stage, mice were taken when hindlimbs were completely paralyzed (average 6 mo of age). Non-ALS control WT $SOD1^{WT}$ mice as well as $C1q^{-/-}$ mice were taken at 6 mo of age (these control mice did not show any symptoms compared with normal nontransgenic mice). Similar tissue collection was done for motor neuron count analysis in end-stage $SOD1^{G93A}$/C3 mice (for end stage, mice were taken when hindlimbs were completely paralyzed as described earlier, at an average of 5 mo of age), with nontransgenic and $C3^{-/-}$ mice at 5 mo of age serving as controls.

Real-Time RT-PCR Analysis of Spinal Cord Inflammation. Total RNA was isolated from freshly dissected and snap-frozen lumbar spinal cords by using the RNeasy Mini Lipid Kit (Qiagen) with DNase treatment. Tissues were homogenized in 1 mL QIAzol Lysis Reagent (Qiagen) using a Polytron homogenizer (IKA-Werke). cDNA was generated from 500 ng of total RNA using SuperScript-III (Invitrogen), and 1/50 was amplified with Power SYBR Green (Applied Biosystems) and 100 nM of each primer in a ABI-7500 real-time PCR machine: one cycle at 50 °C, 2 min; one cycle at 95 °C, 10 min; 40 cycles at 95 °C, 15 s, 60 °C, 1 min. In preliminary experiments, two normalizer genes, mouse γ-actin (*Actg1*) and mouse ribosomal protein S9 (*Rps9*), were analyzed for their variability across all samples. *Rps9* was chosen because of lower variability. The seven mouse candidate genes to be tested (*C1qa*, *C1qb*, *C1qc*, *C3*, *C4*, CD11b/*Itgam*, and *Gfap*) were assessed in several batches but always in parallel with the *Rps9* normalizer (primer sequences are shown in Table S2). All samples to be assessed ($SOD1^{G37R}/C1q^{+/+}$, $SOD1^{G37R}/C1q^{-/-}$, and control $SOD1^{WT}$ spinal cords) were used in parallel. Samples were normalized to *Rps9* and to control $SOD1^{WT}$ mice by using SDS verson 1.4 software (Applied Biosystems) and qBasePlus (Biogazelle; $n = 4$ mice per genotype and disease stage; equally sex-mixed). Statistical significant changes ($P < 0.01$, Student *t* test) were assessed with qBasePlus (Biogazelle) and Prism (GraphPad). Control cDNA samples without reverse transcriptase did not show any significant signal for any of the genes/normalizers tested.

Motor Neuron Counts in Spinal Cords. For tissue collection, mice were perfused with 4% (wt/vol) paraformaldehyde. Spinal cords were cryoprotected and snap-frozen in isopentane in TissueTek (Sakura). Thirty-micrometer serial cryosections were cut between sacral S1 and lumbar L2, and every 24th section was stained with cresyl violet acetate (Sigma). A total of six lumbar L4/L5 sections per animal were analyzed. Total number of large ventral horn motor neurons (diameter >20 μm) were counted bilaterally and averaged per section (average of 28 per section; $n = 4$ mice per genotype and disease stage; equally sex-mixed). Statistical significance ($P < 0.01$, Student *t* test) was assessed with Prism (GraphPad).

Immunohistochemical Analysis of Spinal Cord Inflammation. Mice were perfused with 4% paraformaldehyde, and serial spinal cord cryosections were processed as detailed earlier. Floating sections were incubated in PBS solution/0.3% Triton-X100 overnight at room temperature with the following primary antibodies: polyclonal rabbit antibodies against Iba1/*Aif1* (1:500; Wako), Kv2.1 (1:200; no. 5186; Millipore/Merck) and GFAP (1:4,000; Dako); polyclonal guinea pig antibody against vesicular acetylcholine transferase (VAChT; 1:100; no. 1588, Millipore/Merck); monoclonal rat antibodies against Mac-2/*Lgals3* (1:500; Cedarline). and monoclonal mouse antibodies against synaptotagmin-1/Syt1 (1:500; no. 105011; Synaptic Systems). Primary antibodies for single stainings (Iba1, GFAP, and Mac2) were detected by donkey anti-rabbit and goat anti-rat Cy3 (1:500) coupled secondary antibodies (Jackson ImmunoResearch). For single Syt1 synaptic stainings, primary mouse Syt1 antibodies were detected by donkey anti-rabbit Cy3 (1:500) coupled secondary antibodies (1 h in

PBS solution/0.3% Triton X-100; Jackson ImmunoResearch), followed by NeuroTrace 500/525 (1:100, 20 min in PBS solution; green fluorescent Nissl stain; Invitrogen) to reveal large ventral horn motor neurons. For double VAChT/Kv2.1 pre- and postsynaptic stainings, primary VAChT and Kv2.1 antibodies were detected by highly cross-absorbed goat anti-guinea pig Alexa 488 (1:500) and goat anti-rabbit Alexa 555 (1:500) coupled secondary antibodies (1 h in PBS solution/0.3% Triton X-100; Invitrogen), followed by NeuroTrace 640/660 (1:100, 20 min in PBS solution; far-red fluorescent Nissl stain; Invitrogen) to reveal large ventral horn motor neurons. Control experiments confirmed that the combination of these two secondary antibodies did not produce any cross-reactivity, and confocal parameters were chosen to avoid any spectral bleed-through by using the three fluorescent colors. Analysis was done on a Zeiss Axioimager microscope (for single immunostainings) and an Olympus FV-1000 confocal microscope (for microglial morphology analysis and synaptic density analysis; $n = 4$ mice per genotype and disease stage; equally sex-mixed).

Quantification of Synaptic Density on Ventral Horn Motor Neurons. A fluorescent Nissl stain (as detailed earlier) together with cell size criteria were used to identify large lumbar ventral horn spinal cord motor neurons. For single synaptic density analysis, to determine general presynaptic input, total fluorescence intensity of the presynaptic marker synaptotagmin-1 was measured by using confocal microscopy around NeuroTrace-positive motor neurons (Olympus FV-1000; 60× objectives). Thirty-micrometer serial cryosections were cut between sacral S1 and lumbar L2, and every 24th section was double-stained with NeuroTrace and synaptotagmin-1. We randomly chose approximately 25 to 50 large (>25 μm in diameter) motor neurons, with a clear nuclear staining (as visualized by NeuroTrace) and equally distributed among the six serially collected L4/L5 sections. To analyze the same relative portion of a motor neuron volume, starting from the plane with a clear nuclear stain, we summed the synaptotagmin-1 fluorescence intensities (juxtaposed to the Nissl-positive motor neuron perikarya) within a total of 11 confocal sections (each 0.30 μm thick) along the z axis above (+5 sections) and below (−5 sections) this middle plane, by using ImageJ/Fiji software (with Z-StackProjection/SUM command; National Institutes of Health). Synaptic density was calculated as the total accumulated fluorescent intensity of synaptic stain (relative fluorescence units of synaptotagmin-1 stain) per micrometer of motor neuron contour length (from the largest motor neuron area, which was the starting plane with a clear nuclear stain). For the double-synaptic density analysis, to determine cholinergic C-bouton input, the same strategy as described earlier was used to obtain total fluorescence intensities of individual VAChT pre- and Kv2.1 postsynaptic densities. To determine the amount of VAChT/Kv2.1 apposition/colocalization in the analyzed C-boutons, ImageJ/Fiji was used to find overlapping signals (with ImageCalculator/ADD command) and a ratio of apposed/colocalized VAChT/Kv2.1 to combined total VAChT and Kv2.1 signals calculated. To assess a potential general reduction of perikaryal VAChT signal within large surviving motor neurons, the diffuse, grainy VAChT fluorescence intensity present within the NeuroTrace (fluorescent Nissl stain) positive perikarya was measured and designated "perVAChT." This VAChT-fluorescence intensity was clearly distinguishable from the bouton-like VAChT-positive fluorescence signal of the presynaptic densities, juxtaposed onto the motor neuron perikarya and designated "synVAChT." To determine the motor neuron diameter, the largest neuronal area with a clear nuclear stain, as defined by NeuroTrace positive fluorescent Nissl staining, was used and disease related shrinkage of motor neuronal size assessed. All statistical differences ($P < 0.01$; Student t test) were calculated, and graphs were plotted by Prism ($n = 4$ mice per genotype and disease stage; equally sex-mixed).

1. Lobsiger CS, Boillée S, Cleveland DW (2007) Toxicity from different SOD1 mutants dysregulates the complement system and the neuronal regenerative response in ALS motor neurons. *Proc Natl Acad Sci USA* 104(18):7319–7326.
2. Botto M, et al. (1998) Homozygous C1q deficiency causes glomerulonephritis associated with multiple apoptotic bodies. *Nat Genet* 19(1):56–59.
3. Mitchell DA, et al. (2002) C1q deficiency and autoimmunity: The effects of genetic background on disease expression. *J Immunol* 168(5):2538–2543.
4. Lobsiger CS, Garcia ML, Ward CM, Cleveland DW (2005) Altered axonal architecture by removal of the heavily phosphorylated neurofilament tail domains strongly slows superoxide dismutase 1 mutant-mediated ALS. *Proc Natl Acad Sci USA* 102(29): 10351–10356.
5. Lobsiger CS, et al. (2009) Schwann cells expressing dismutase active mutant SOD1 unexpectedly slow disease progression in ALS mice. *Proc Natl Acad Sci USA* 106(11): 4465–4470.

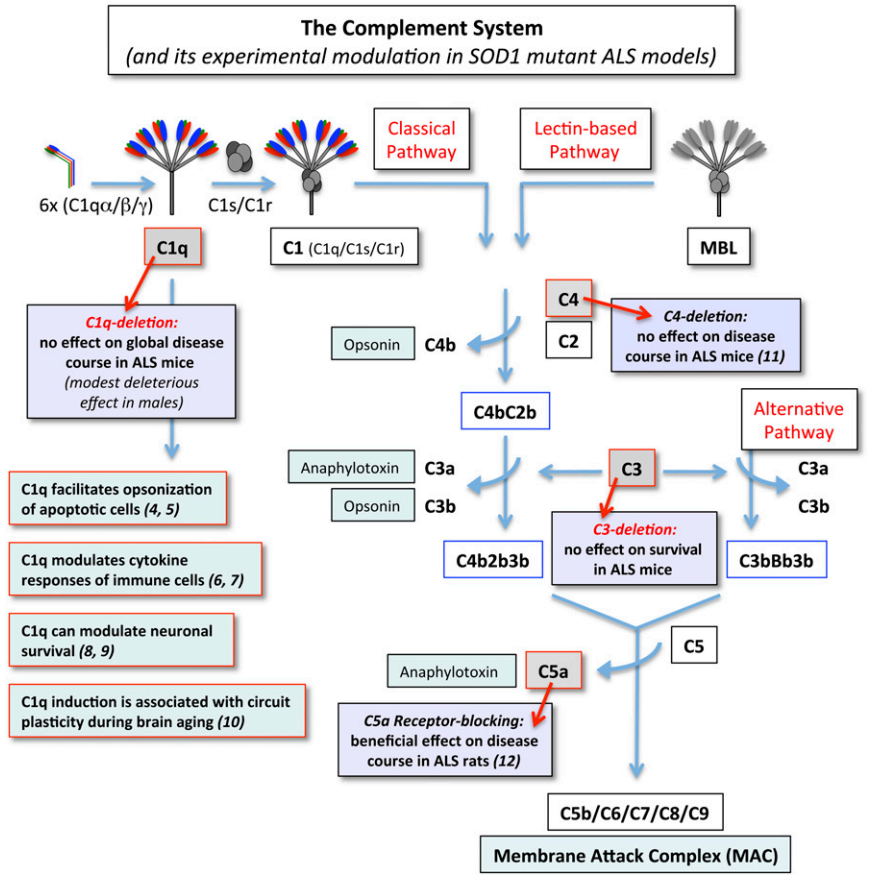

Fig. S1. Complement system and its experimental modulation in ALS models. Overview of the three different complement activation pathways: classical, lectin-based, and alternative (1, 2). For the classical pathway, C1q is the initiating component. C1q forms a Y-shaped heteromultimer consisting of six obligate heterotrimers formed by the three C1q α-, β-, and γ-chains (encoded by the *C1qa*, *C1qb*, and *C1qc* genes). The two proteases C1r and C1s are associated with the stalk of C1q, forming the mature C1 complex that gets activated by aggregated immune complexes. C1q can also act independent of associated C1s/r (and downstream complement activation) via several proposed C1q receptors (3) (see text). As such, C1q can recognize apoptotic cells (neurons) to enhance clearance by phagocytes (microglia) (4, 5), act on immune cells (microglia) to modulate their cytokine release (6, 7), and have direct protective actions on neurons (8, 9), and increasing C1q protein levels were associated with functions during normal brain aging (10) (see text). Indicated are the studies that so far have assessed the contribution of different complement components in ALS models (C1q/C3 detailed in present study; C4 detailed in ref. 11; C5a detailed in ref. 12). Anaphylotoxins modulate immune cells. Opsonins facilitate phagocytosis. "ALS mice/rats" indicates mutant SOD1-linked mouse and rat models. MBL, mannose binding lectin.

1. Veerhuis R, Nielsen HM, Tenner AJ (2011) Complement in the brain. *Mol Immunol* 48(14):1592–1603.
2. Bohlson SS, Fraser DA, Tenner AJ (2007) Complement proteins C1q and MBL are pattern recognition molecules that signal immediate and long-term protective immune functions. *Mol Immunol* 44(1-3):33–43.
3. Nayak A, Ferluga J, Tsolaki AG, Kishore U (2010) The non-classical functions of the classical complement pathway recognition subcomponent C1q. *Immunol Lett* 131(2):139–150.
4. Fraser DA, Laust AK, Nelson EL, Tenner AJ (2009) C1q differentially modulates phagocytosis and cytokine responses during ingestion of apoptotic cells by human monocytes, macrophages, and dendritic cells. *J Immunol* 183(10):6175–6185.
5. Fraser DA, Pisalyaput K, Tenner AJ (2010) C1q enhances microglial clearance of apoptotic neurons and neuronal blebs, and modulates subsequent inflammatory cytokine production. *J Neurochem* 112(3):733–743.
6. Färber K, et al. (2009) C1q, the recognition subcomponent of the classical pathway of complement, drives microglial activation. *J Neurosci Res* 87(3):644–652.
7. Benoit ME, Clarke EV, Morgado P, Fraser DA, Tenner AJ (2012) Complement protein C1q directs macrophage polarization and limits inflammasome activity during the uptake of apoptotic cells. *J Immunol* 188(11):5682–5693.
8. Humphries MM, et al. (2012) C1q enhances cone photoreceptor survival in a mouse model of autosomal recessive retinitis pigmentosa. *Eur J Hum Genet* 20(1):64–68.
9. Benoit ME, Tenner AJ (2011) Complement protein C1q-mediated neuroprotection is correlated with regulation of neuronal ***gene*** and microRNA expression. *J Neurosci* 31(9):3459–3469.
10. Stephan AH, et al. (2013) A dramatic increase of C1q Protein in the CNS during normal aging. *J Neurosci* 33(33):13460–13474.
11. Chiu IM, et al. (2009) Activation of innate and humoral immunity in the peripheral nervous system of ALS transgenic mice. *Proc Natl Acad Sci USA* 106(49):20960–20965.
12. Woodruff TM, et al. (2008) The complement factor C5a contributes to pathology in a rat model of amyotrophic lateral sclerosis. *J Immunol* 181(12):8727–8734.

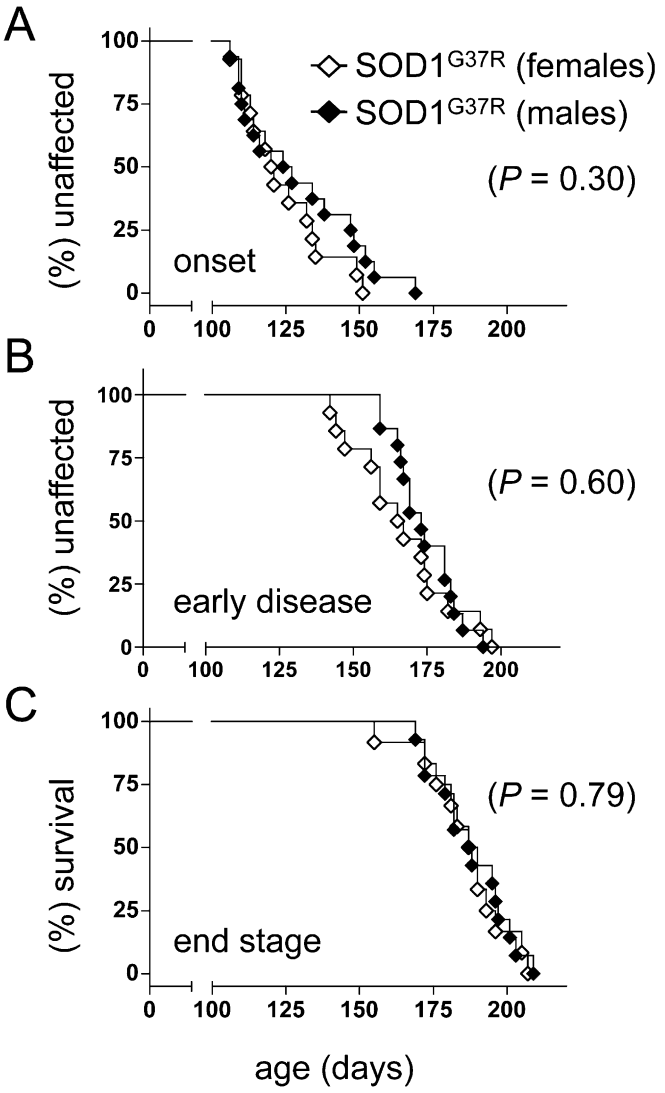

Fig. S2. Disease course in SOD1^{G37R}/C1q$^{+/+}$ mutant ALS mice is sex-independent. (*A–C*) Data from the same cohort of mice as in Fig. 6 was plotted sex-separated, using only mutant ALS mice (SOD1^{G37R}) with normal C1q content (SOD1^{G37R}/C1q$^{+/+}$). Shown are Kaplan–Meier plots of ages (in days) at which disease onset (weight peak) (*A*), early disease (10% weight loss) (*B*), or end stage (paralysis) (*C*) were reached in female (open diamonds) or male (filled diamonds) mutant SOD1^{G37R} ALS mice with normal C1q content. No statistically significant differences between sexes were detected [$P = 0.30$ (*A*), $P = 0.60$ (*B*), $P = 0.79$ (*C*), log-rank and Student *t* tests; Table S1)].

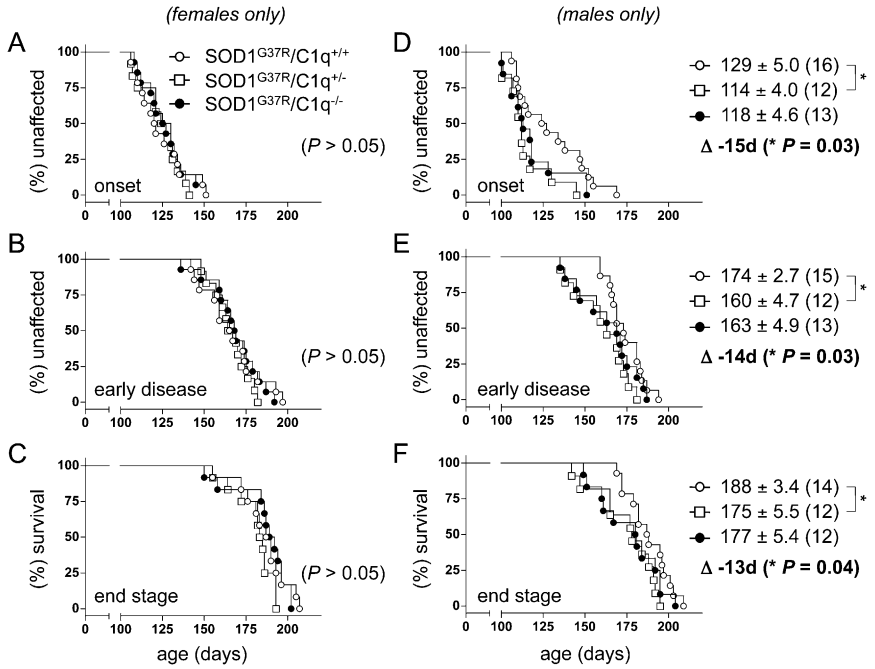

Fig. S3. Modest protective effect of C1q induction on disease course in male ALS mice. (*A–F*) The initial cohort (Fig. 6) was plotted sex-separated (detailed in Table S1). Shown are Kaplan–Meier plots of ages (in days) at which onset (weight peak) (*A* and *D*), early disease (10% weight loss) (*B* and *E*), or end stage (paralysis) (*C* and *F*) were reached in female (*A–C*) or male (*D–F*) mutant SOD1^{G37R} mice with normal (C1q$^{+/+}$, ○), heterozygous (C1q$^{+/-}$, □) or full deletion (C1q$^{-/-}$, ●) of C1q. Average (±SEM) ages (in days) of the different disease stages are shown, and animal numbers are indicated in brackets. Heterozygous or homozygous C1q deletion did not change disease in female ALS mice (*A–C*) ($P > 0.05$; log-rank and Student *t* tests; Table S1), but led to earlier onset and reduced survival in males (*D–F*), reaching statistical significance for heterozygous C1q-deleted ALS males [SOD1^{G37R}/C1q$^{+/-}$ mice; $*P = 0.03$ (*D*), $*P = 0.03$ (*E*), and $*P = 0.04$ (*F*), log-rank and Student *t* tests; Table S1], whereas complete C1q deletion (SOD1^{G37R}/C1q$^{-/-}$ mice) showed the same trend without reaching significance [$P = 0.13$ (*D*), $P = 0.27$ (*E*), $P = 0.18$ (*F*), log-rank and Student *t* tests; Table S1].

Table S1. Average ages of Kaplan–Meier plots for disease onset, early disease, and end stage in ALS mice with normal, reduced, or deleted C1q content

Mice	Onset (weight peak)	Early disease (10% weight loss)	End stage (paralysis)
Sex-mixed			
SOD1^{G37R}/C1q$^{+/+}$	127 ± 3.2 ($n = 30$)	170 ± 2.6 ($n = 29$)	187 ± 2.6 ($n = 26$)
SOD1^{G37R}/C1q$^{+/-}$	120 ± 2.8 ($n = 24$)	163 ± 2.8 ($n = 24$)	178 ± 3.2 ($n = 24$)
SOD1^{G37R}/C1q$^{-/-}$	122 ± 2.9 ($n = 27$)	166 ± 3.1 ($n = 27$)	181 ± 3.6 ($n = 24$)
Females only			
SOD1^{G37R}/C1q$^{+/+}$	124 ± 3.8 ($n = 14$)	167 ± 4.5 ($n = 14$)	186 ± 4.2 ($n = 12$)
SOD1^{G37R}/C1q$^{+/-}$	125 ± 3.4 ($n = 12$)	166 ± 3.1 ($n = 12$)	181 ± 3.4 ($n = 12$)
SOD1^{G37R}/C1q$^{-/-}$	126 ± 3.4 ($n = 14$)	169 ± 4.0 ($n = 14$)	186 ± 4.7 ($n = 12$)
Males only			
SOD1^{G37R}/C1q$^{+/+}$	129 ± 5.0 ($n = 16$)	174 ± 2.7 ($n = 15$)	188 ± 3.4 ($n = 14$)
SOD1^{G37R}/C1q$^{-/-}$	118 ± 4.6 ($n = 13$)	163 ± 4.9 ($n = 13$)	177 ± 5.4 ($n = 12$)
Δ, days	−11 ($P = 0.13$)	−11 ($P = 0.27$)	−11 ($P = 0.18$)
Males only			
SOD1^{G37R}/C1q$^{+/+}$	129 ± 5.0 ($n = 16$)	174 ± 2.7 ($n = 15$)	188 ± 3.4 ($n = 14$)
SOD1^{G37R}/C1q$^{+/-}$	114 ± 4.0 ($n = 12$)	160 ± 4.7 ($n = 12$)	175 ± 5.5 ($n = 12$)
Δ, days	−15 ($P = 0.03$)	−14 ($P = 0.03$)	−13 ($P = 0.04$)

Table S2. Primer sequences for quantitative RT-PCR analysis with indicated genomic position and amplicon sizes

Gene	Quantitative PCR primer sequence	Amplicon size, bp	Amplicon position
C1qa forward	5′-CGGGTCTCAAAGGAGAGAGA-3′	192	Over intron
C1qa reverse	5′-TATTGCCTGGATTGCCTTTC-3′		
C1qb forward	5′-CAGGGATAAAGGGGGAGAAA-3′	195	Over intron
C1qb reverse	5′-TCTGTGTAGCCCCGTAGTCC-3′		
C1qc forward	5′-CTTCTGGCCCTACCACTCAG-3′	171	Over intron
C1qc reverse	5′-CTTCTGACCCTTGGGTCCTC-3′		
C4 forward	5′-CAGGACAGAACAGTGGAGCA-3′	168	Over intron
C4 reverse	5′-ATCTTCAGCACGAAGGCAGT-3′		
C3 forward	5′-CCAGGAGTGAATTGGAGGAA-3′	167	Over intron
C3 reverse	5′-CCAGGTGGTGATGGAATCTT-3′		
cd11b forward	5′-CATCTGCCAAGACGATCTCA-3′	186	Over intron
cd11b reverse	5′-TTCTGGCTTGCTGAATCCTT-3′		
Gfap forward	5′-CACGAACGAGTCCCTAGAGC-3′	234	Over intron
Gfap reverse	5′-ATGGTGATGCGGTTTTCTTC-3′		
Rps9 forward	5′-GACCAGGAGCTAAAGTTGATTGGA-3′	112	Over intron
Rps9 reverse	5′-GCGTCAACAGCTCCCGGGC-3′		
Actg1 forward	5′-TGGATCAGCAAGCAGGAGTATG-3′	77	In exon
Actg1 reverse	5′-CCTGCTCAGTCCATCTAGAAGCA-3′		